Bilinear Time-Frequency Representations of Signals: The Shift-Scale Invariant Class

Franz Hlawatsch, *Member, IEEE,* and Rüdiger L. Urbanke

***Abstract*— We consider the class of bilinear time-frequency representations (BTFR's) that are invariant (or covariant) to time shifts, frequency shifts, and time-frequency scalings. This "shift-scale invariant" class is the intersection of the classical shift-invariant (Cohen) class and the recently defined affine class. The mathematical description of shift-scale invariant BTFR's is in terms of a 1-D kernel and is thus particularly simple. The paper concentrates on the time-frequency localization properties of shift-scale invariant BTFR's. Since any shift-scale invariant BTFR is a superposition of generalized Wigner distributions, the time-frequency localization of the family of generalized Wigner distributions is studied first. For those shift-scale invariant BTFR's that may be interpreted as smoothed versions of the Wigner distribution (e.g., the Choi–Williams distribution), an analysis in the Fourier transform domain shows interesting peculiarities regarding time-frequency concentration and interference geometry properties.**

I. Introduction

JOINT time-frequency representations of signals combine time- and frequency-domain analyses by displaying a signal as a function defined over a joint time-frequency plane. In most cases, the goal is to characterize the temporal localization of spectral components. Time-frequency representations have been shown to be useful for a number of applications in a variety of different areas. A tutorial discussion may be found, e.g., in [1].

This paper considers bilinear time-frequency representations (BTFR's) with "energetic" interpretation like the Wigner distribution or the spectrogram [2]. These BTFR's will be written as $T_{x,y}(t,f)$, where $x(t)$ and $y(t)$ are two signals, and t and f denote time and frequency, respectively. The (quadratic) "autorepresentation" $T_x(t,f)$ of a single signal $x(t)$ is defined by letting $y(t) = x(t)$, i.e., $T_x(t,f) \triangleq T_{x,x}(t,f)$.

A. The Shift-Invariant Class and the Affine Class

Two major BTFR classes have been defined in the literature based on invariance (or "covariance") properties with respect to the time-shift operator $\mathbf{S}_\tau$, the frequency-shift (modulation) operator $\mathbf{M}_u$, and the time-frequency scaling operator $\mathbf{C}_a$ defined as

$$(\mathbf{S}_\tau x)(t) = x(t-\tau)$$
$$(\mathbf{M}_\upsilon x)(t) = x(t)e^{j2\pi\upsilon t}$$
$$(\mathbf{C}_a x)(t) = \sqrt{|a|}x(at), \quad a \neq 0.$$

(i) The classical *shift-invariant class* or *Cohen class* $\mathcal{C}$ [1]–[4] comprises all BTFR's T that are "invariant" to time and frequency shifts

$$T \in \mathcal{C} \quad \text{if} \quad T_{\mathbf{M}_\upsilon \mathbf{S}_\tau x, \mathbf{M}_\upsilon \mathbf{S}_\tau y}(t,f) = T_{x,y}(t-\tau, f-\upsilon). \tag{1.1}$$

(ii) More recently, the *affine class* $\mathcal{A}$ has been defined as the class of all BTFR's T that are "invariant" to time shifts and time-frequency scalings [5], [6]

$$T \in \mathcal{A} \quad \text{if} \quad T_{\mathbf{S}_\tau \mathbf{C}_a x, \mathbf{S}_\tau \mathbf{C}_a y}(t,f) = T_{x,y}\left(a(t-\tau), \frac{f}{a}\right). \tag{1.2}$$

B. The Shift-Scale Invariant Class

In this paper, we concentrate on a class $\mathcal{D}$ of BTFR's, which is called the *shift-scale invariant class* [2], whose members simultaneously satisfy the axioms of both the classes $\mathcal{C}$ and $\mathcal{A}$. Hence, this class is defined by combining (1.1) and (1.2) as follows:

$T \in \mathcal{D}$ if

$$T_{\mathbf{M}_\upsilon \mathbf{S}_\tau \mathbf{C}_a x, \mathbf{M}_\upsilon \mathbf{S}_\tau \mathbf{C}_a y}(t,f) = T_{x,y}\left(a(t-\tau), \frac{f-\upsilon}{a}\right).$$

Members of the shift-scale invariant class $\mathcal{D}$ are "invariant" to time shifts, frequency shifts, and time-frequency scalings. Evidently, $\mathcal{D}$ is a subclass of both the shift-invariant class $\mathcal{C}$ and the affine class $\mathcal{A}$; in fact, it is the intersection of $\mathcal{C}$ and $\mathcal{A}$

$$\mathcal{D} = \mathcal{C} \cap \mathcal{A}.$$

This is illustrated in Fig. 1, which also depicts some specific BTFR's contained in $\mathcal{C}$, $\mathcal{A}$, and $\mathcal{D}$. In particular, the shift-scale invariant class $\mathcal{D}$ contains the *Wigner distribution* (WD) [7], [8], the *Rihaczek distribution* (see Part III of [7] and [8]), the families of *generalized Wigner distributions* and *real-valued generalized Wigner distributions* (see Part III of [7] and [8], [9]), the *Born-Jordan distribution* [10], and the *Choi-Williams distribution* [11]. Members of the shift-invariant class $\mathcal{C}$ that are not scale invariant (and thus outside $\mathcal{D}$) are the *spectrogram* (see Part III of [7] and [8], [12], [13]), the *Page distribution* [14] and *Levin distribution* [15], and various

Manuscript received February 5, 1992; revised January 13, 1993. The associate editor coordinating the review of this paper and approving it for publication was Prof. Miguel A. Lagunas. This work was supported by the Fonds zur Förderung der wissenschaftlichen Forschung under Grants P7354-PHY and J0530-TEC.

F. Hlawatsch is with the Institut für Nachrichtentechnik und Hochfrequenztechnik, Technische Universität Wien, Vienna, Austria.

R. L. Urbanke is with the Department of Electrical Engineering, Washington University, St. Louis, MO 63130.

IEEE Log Number 9214193.

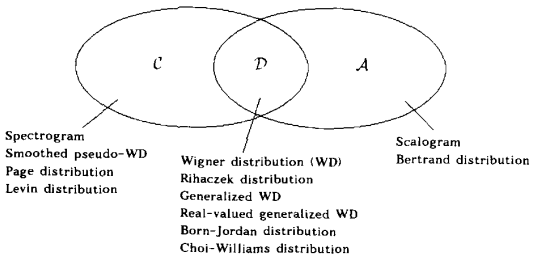

Fig. 1. Shift-invariant class $\mathcal{C}$, the affine class $\mathcal{A}$, and the shift-scale invariant class $\mathcal{D} = \mathcal{C} \cap \mathcal{A}$

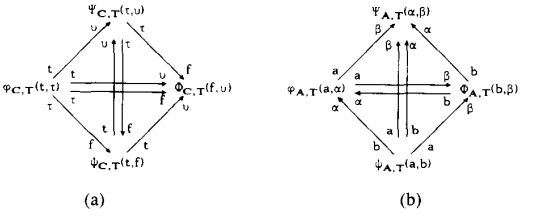

Fig. 2. Fourier transform relations connecting (a) the kernels of the shift-invariant class $\mathcal{C}$; (b) the kernels of the affine class $\mathcal{A}$.

smoothed versions of the WD such as the *smoothed pseudo-Wigner distribution* [8], [16], [17]. Finally, members of the affine class $\mathcal{A}$ that are not frequency-shift invariant (and thus outside $\mathcal{D}$) are the *scalogram* [5] and the *Bertrand distribution* [5], [6].

The shift-scale invariant class $\mathcal{D}$ is interesting for several reasons:

(i) It forms the intersection of the two major BTFR classes defined so far, and its members satisfy three important invariance properties.

(ii) It permits a particularly simple mathematical description: Whereas BTFR's of either $\mathcal{C}$ or $\mathcal{A}$ are generally characterized in terms of a 2-D kernel function, we shall show that BTFR's of $\mathcal{D}$ can be characterized by a 1-D kernel function.

(iii) It provides a basis for implementing a specific *smoothing of the WD*, which results in a partial attenuation of the WD's cross or interference terms and yet retains some of the WD's nice mathematical properties.

While the first two points are mainly theoretical, the last point is potentially important for practical signal analysis applications. The *Choi-Williams distribution* [11], which has received some attention over the past few years, is an example for the type of smoothing featured by some BTFR's of the shift-scale invariant class $\mathcal{D}$.

C. Survey of Paper

The paper is organized as follows. Section II reviews the mathematical description of the classes $\mathcal{C}$ and $\mathcal{A}$ in terms of 2-D kernel functions and specializes this description to the shift-scale invariant class $\mathcal{D}$. Section III studies the family of *generalized WD's*, which can be viewed as the basic BTFR's of $\mathcal{D}$. The specific type of WD smoothing featured by certain BTFR's of $\mathcal{D}$ is finally considered in Section IV.

While Section II is of a more formal nature, Sections III and IV emphasize the time-frequency localization properties of the BTFR's, which are of major importance in practical applications. The central question here is: "How will a given BTFR look like for a given signal?" Regarding this question, two relevant BTFR properties are a BTFR's *time-frequency concentration* and *interference geometry* [8], [18]. These properties are studied by means of simple but typical examples.

II. The Shift-Scale Invariant Class

Since the shift-scale invariant class $\mathcal{D}$ is the intersection of the shift-invariant class $\mathcal{C}$ and the affine class $\mathcal{A}$, the mathematical description of BTFR's of $\mathcal{D}$ can be derived by specializing either the description of $\mathcal{C}$ or that of $\mathcal{A}$.

A. Description of Shift-Invariant BTFR's and Affine BTFR's

We start by reviewing the description of the shift-invariant class $\mathcal{C}$. It is well known (e.g., [2]) that any BTFR $T \in \mathcal{C}$ may be written as

$$T_{x,y}(t,f) = \int_{t'}\int_{\tau} \varphi_{C,T}(t-t',\tau) q_{x,y}(t',\tau) e^{-j2\pi f\tau} dt' d\tau \tag{2.1.a}$$

$$= \int_{f'}\int_{\upsilon} \Phi_{C,T}(f-f',\upsilon) Q_{x,y}(f',\upsilon) e^{j2\pi t\upsilon} df' d\upsilon \tag{2.1.b}$$

$$= \int_{t'}\int_{f'} \psi_{C,T}(t-t',f-f') W_{x,y}(t',f') dt' df' \tag{2.1.c}$$

$$= \int_{\tau}\int_{\upsilon} \Psi_{C,T}(\tau,\upsilon) A_{x,y}(\tau,\upsilon) e^{j2\pi(t\upsilon - f\tau)} d\tau d\upsilon, \tag{2.1.d}$$

where the time-domain signal product $q_{x,y}(t,\tau)$, the frequency-domain signal product $Q_{x,y}(f,\upsilon)$, the WD $W_{x,y}(t,f)$, and the ambiguity function (AF) $A_{x,y}(\tau,\upsilon)$ are defined as

$$q_{x,y}(t,\tau) = x\Big(t+\frac{\tau}{2}\Big) y^*\Big(t-\frac{\tau}{2}\Big),$$

$$Q_{x,y}(f,\upsilon) = X\Big(f+\frac{\upsilon}{2}\Big) Y^*\Big(f-\frac{\upsilon}{2}\Big),$$

$$W_{x,y}(t,f) = \int_{\tau} x\Big(t+\frac{\tau}{2}\Big) y^*\Big(t-\frac{\tau}{2}\Big) e^{-j2\pi f\tau} d\tau,$$

$$A_{x,y}(\tau,\upsilon) = \int_{t} x\Big(t+\frac{\tau}{2}\Big) y^*\Big(t-\frac{\tau}{2}\Big) e^{-j2\pi\upsilon t} dt.$$

These four signal representations are seen to be interrelated by Fourier transforms. It is shown in Fig. 2(a) that the same Fourier transforms connect the 2-D kernel functions $\varphi_{C,T}(t,\tau)$, $\Phi_{C,T}(f,\upsilon)$, $\psi_{C,T}(t,f)$, and $\Psi_{C,T}(\tau,\upsilon)$. Each of the kernel functions $\varphi_{C,T}(t,\tau)$ etc. uniquely characterizes the BTFR T.

In a similar manner, any affine BTFR $T \in \mathcal{A}$ can be written as [5], [6]

$$T_{x,y}(t,f) = |f| \int_{t'} \int_{\tau} \varphi_{A,T}(f(t-t'), f\tau) q_{x,y}(t',\tau) dt' d\tau \quad (2.2.a)$$

$$= \frac{1}{|f|} \int_{f'} \int_{\upsilon} \Phi_{A,T}\left(\frac{f'}{f}, \frac{\upsilon}{f}\right) Q_{x,y}(f',\upsilon) e^{j2\pi t\upsilon} df' d\upsilon \quad (2.2.b)$$

$$= \int_{t'} \int_{f'} \psi_{A,T}\left(f(t-t'), \frac{f'}{f}\right) W_{x,y}(t',f') dt' df' \quad (2.2.c)$$

$$= \int_{\tau} \int_{\upsilon} \Psi_{A,T}\left(f\tau, \frac{\upsilon}{f}\right) A_{x,y}(\tau,\upsilon) e^{j2\pi t\upsilon} d\tau d\upsilon, \quad (2.2.d)$$

where the kernel functions $\varphi_{A,T}(a,\alpha)$, $\Phi_{A,T}(b,\beta)$, $\psi_{A,T}(a,b)$, and $\Psi_{A,T}(\alpha,\beta)$ are interrelated by Fourier transforms according to Fig. 2(b). Again, each of these kernel functions characterizes the BTFR T.

B. Description of Shift-Scale Invariant BTFR's

Let us now consider the shift-scale invariant class $\mathcal{D} = \mathcal{C} \cap \mathcal{A}$. Since a shift-scale invariant BTFR $T \in \mathcal{D}$ is a member of both $\mathcal{C}$ and $\mathcal{A}$, it is clear that both sets of general forms (2.1) and (2.2) can be used in this case.

1) Using the class-$\mathcal{C}$ description (2.1), it is easily shown that the additional axiom of scale invariance constrains the kernels $\varphi_{C,T}(t,\tau)$, $\Phi_{C,T}(f,\upsilon)$, $\psi_{C,T}(t,f)$, and $\Psi_{C,T}(\tau,\upsilon)$ to assume the following special forms [2]:

$$\varphi_{C,T}(t,\tau) = \frac{1}{|\tau|} g_T\left(\frac{t}{\tau}\right) \quad (2.3.a)$$

$$\Phi_{C,T}(f,\upsilon) = \frac{1}{|\upsilon|} g_T\left(-\frac{f}{\upsilon}\right) \quad (2.3.b)$$

$$\psi_{C,T}(t,f) = \int_{\eta} g_T(\eta) \frac{1}{|\eta|} \exp\left(-j2\pi \frac{tf}{\eta}\right) d\eta \quad (2.3.c)$$

$$\Psi_{C,T}(\tau,\upsilon) = G_T(\tau\upsilon), \quad (2.3.d)$$

where $G_T(\xi)$ is the Fourier transform of $g_T(\eta)$

$$G_T(\xi) = \int_{\eta} g_T(\eta) e^{-j2\pi\xi\eta} d\eta.$$

Note that a 1-D "kernel function" ($g_T(\eta)$ or, equivalently, $G_T(\xi)$) is sufficient to uniquely characterize a shift-scale invariant BTFR. In addition, it is important to notice that $\Psi_{C,T}(\tau,\upsilon)$ as given by (2.3.d) is a function of the *product* $\tau\upsilon$. Similarly, $\psi_{C,T}(t,f)$ is a function of the product tf.

2) Using the framework of the class-$\mathcal{A}$ description (2.2), it is easily shown that the additional axiom of frequency-shift invariance constrains the kernels $\varphi_{A,T}(a,\alpha)$, $\Phi_{A,T}(b,\beta)$, $\psi_{A,T}(a,b)$, and $\Psi_{A,T}(\alpha,\beta)$ of a shift-scale invariant BTFR to assume the following special forms:

$$\varphi_{A,T}(a,\alpha) = \frac{1}{|\alpha|} g_T\left(\frac{a}{\alpha}\right) e^{-j2\pi\alpha} \quad (2.4.a)$$

$$\Phi_{A,T}(b,\beta) = \frac{1}{|\beta|} g_T\left(-\frac{1-b}{\beta}\right) \quad (2.4.b)$$

TABLE I
DESIRABLE BTFR PROPERTIES AND THE CORRESPONDING CONSTRAINTS ON THE KERNEL $g_T(\eta)$ OR $G_T(\xi)$. (The shift-invariance and scale-invariance properties are always satisfied.)

BTFR PROPERTY	KERNEL CONSTRAINT
P_1: Real-valued auto-BTFR $T_x(t,f) \in \mathbb{R}$	$G_T(\xi) \in \mathbb{R}$
P_2: Marginal properties $\int_f T_x(t,f)\,df = \lvert x(t)\rvert^2$, $\int_t T_x(t,f)\,dt = \lvert X(f)\rvert^2$	$G_T(0) = 1$
P_3: Instantaneous frequency/ group delay properties $\frac{\int f T_x(t,f)\,df}{\int T_x(t,f)\,df} = f_{x,\mathrm{inst}}(t)$, $\frac{\int t T_x(t,f)\,dt}{\int T_x(t,f)\,dt} = t_{x,\mathrm{group}}(f)$	$G_T(0) = 1$ and $\frac{d}{d\xi} G_T(\xi)\big\rvert_{\xi=0} = 0$
P_4: Finite-support properties $x(t)=0$ for $t \notin [t_1,t_2] \Rightarrow T_x(t,f)=0$ for $t \notin [t_1,t_2]$ $X(f)=0$ for $f \notin [f_1,f_2] \Rightarrow T_x(t,f)=0$ for $f \notin [f_1,f_2]$	$g_T(\eta)=0$ for $\lvert\eta\rvert > 1/2$
P_5: Moyal's formula (unitarity) $(T_{x_1,y_1}, T_{x_2,y_2}) = (x_1,x_2)(y_1,y_2)^*$	$\lvert G_T(\xi)\rvert = 1$
P_6: Convolution/multiplication property $y(t) = \int_{t'} h(t-t')x(t')\,dt' \Rightarrow$ $T_y(t,f) = \int_{t'} T_h(t-t',f)\, T_x(t',f)\,dt'$ $y(t) = h(t)\,x(t) \Rightarrow$ $T_y(t,f) = \int_{f'} T_h(t,f-f')\, T_x(t,f')\,df'$	$G_T(\xi) = e^{c\xi}$, $c \in \mathbb{C}$

$$\psi_{A,T}(a,b) = \int_{\eta} g_T(\eta) \frac{1}{|\eta|} \exp\left(-j2\pi \frac{a(1-b)}{\eta}\right) d\eta \quad (2.4.c)$$

$$\Psi_{A,T}(\alpha,\beta) = G_T(\alpha\beta) e^{-j2\pi\alpha}, \quad (2.4.d)$$

where $g_T(\eta)$ and $G_T(\xi)$ are the same as before. It follows by comparison of (2.3) and (2.4) that for a shift-scale invariant BTFR T, the class-$\mathcal{C}$ kernels $\varphi_{C,T}(t,\tau)$, $\Phi_{C,T}(f,\upsilon)$, $\psi_{C,T}(t,f)$, and $\Psi_{C,T}(\tau,\upsilon)$ on the one hand and the class-$\mathcal{A}$ kernels $\varphi_{A,T}(a,\alpha)$, $\Phi_{A,T}(b,\beta)$, $\psi_{A,T}(a,b)$, and $\Psi_{A,T}(\alpha,\beta)$ on the other are related as

$$\varphi_{A,T}(a,\alpha) = \varphi_{C,T}(a,\alpha) e^{-j2\pi\alpha}$$
$$\Phi_{A,T}(b,\beta) = \Phi_{C,T}(1-b,\beta)$$
$$\psi_{A,T}(a,b) = \psi_{C,T}(a,1-b)$$
$$\Psi_{A,T}(\alpha,\beta) = \Psi_{C,T}(\alpha,\beta) e^{-j2\pi\alpha}.$$

An important result of the above discussion is the fact that a shift-scale invariant BTFR can be characterized by a 1-D kernel function. It is easily shown that the BTFR T will satisfy a number of desirable mathematical properties if its kernel $g_T(\eta)$ (or, equivalently, $G_T(\xi)$) meets certain very simple constraints. Some BTFR properties and the corresponding constraints are summarized in Table I [19], [20], [1]. (Note that the properties of time-shift invariance, frequency-shift invariance, and time-frequency scale invariance are automatically satisfied.) Table II lists some specific shift-scale invariant BTFR's, their kernels, and the properties they satisfy.

TABLE II
SOME SHIFT-SCALE INVARIANT BTFR'S

BTFR	DEFINITION	KERNELS	PROPERTIES
Wigner distribution	$W_{x,y}(t,f) = \int_\tau x(t+\frac{\tau}{2})y^*(t-\frac{\tau}{2})e^{-j2\pi f\tau}d\tau$	$g_W(\eta)=\delta(\eta)$ $G_W(\xi)=1$	P_1 - P_6
Rihaczek distribution	$R_{x,y}(t,f) = X(f)\,y^*(t)\,e^{j2\pi tf}$	$g_R(\eta)=\delta(\eta+\frac{1}{2})$ $G_R(\xi)=e^{j\pi\xi}$	P_2; P_4-P_6
Generalized Wigner distribution	$W^{(\rho)}_{x,y}(t,f) = \int_\tau x[t+(\frac{1}{2}+\rho)\tau]\,y^*[t-(\frac{1}{2}-\rho)\tau]e^{-j2\pi f\tau}d\tau$	$g_{W(\rho)}(\eta)=\delta(\eta+\rho)$ $G_{W(\rho)}(\xi)=e^{j2\pi\rho\xi}$	P_2, P_5, P_6 P_4 for $\lvert\rho\rvert<\frac{1}{2}$ P_1, P_3 for $\rho=0$
Real-valued generalized Wigner distribution	$RW^{(\rho)}_{x,y}(t,f) = \frac{1}{2}[W^{(\rho)}_{x,y}(t,f)+W^{(-\rho)}_{x,y}(t,f)]$	$g_{RW(\rho)}(\eta) = \frac{1}{2}[\delta(\eta+\rho)+\delta(\eta-\rho)]$ $G_{RW(\rho)}(\xi)=\cos(2\pi\rho\xi)$	P_1-P_3 P_4 for $\lvert\rho\rvert<\frac{1}{2}$ P_5, P_6 for $\rho=0$
Born-Jordan distribution	$BJD_{x,y}(t,f) = \int\frac{1}{\lvert\tau\rvert}\left[\int_{t-\lvert\tau\rvert/2}^{t+\lvert\tau\rvert/2} x(t'+\frac{\tau}{2}) \times y^*(t'-\frac{\tau}{2})dt'\right]e^{-j2\pi f\tau}d\tau$	$g_{BJD}(\eta) = \begin{cases}1, & \lvert\eta\rvert<1/2\\ 0, & \lvert\eta\rvert>1/2\end{cases}$ $G_{BJD}(\xi)=\frac{\sin(\pi\xi)}{\pi\xi}$	P_1-P_4
Choi-Williams distribution	$CWD_{x,y}(t,f) = \int\frac{1}{\lvert\tau\rvert}\left[\int_{t'}\sqrt{\frac{\sigma}{4\pi}}e^{-\frac{\sigma}{4}(\frac{t-t'}{\tau})^2} \times x(t'+\frac{\tau}{2})y^*(t'-\frac{\tau}{2})dt'\right]e^{-j2\pi f\tau}d\tau$	$g_{CWD}(\eta)=\sqrt{\frac{\sigma}{4\pi}}e^{-\frac{\sigma}{4}\eta^2}$ $G_{CWD}(\xi)=e^{-(2\pi\xi)^2/\sigma}$	P_1-P_3

III. The Generalized WD

In this section, we study the *generalized WD* (GWD), which is a specific family of shift-scale invariant BTFR's. The GWD is defined as

$$W^{(\rho)}_{x,y}(t,f) = \int_\tau x\left[t+\left(\frac{1}{2}+\rho\right)\tau\right]y^*\left[t-\left(\frac{1}{2}-\rho\right)\tau\right]e^{-j2\pi f\tau}d\tau = \int_v X\left[f+\left(\frac{1}{2}-\rho\right)v\right]Y^*\left[f-\left(\frac{1}{2}+\rho\right)v\right]e^{j2\pi tv}dv$$

where ρ is a real-valued parameter (see Part III of [7] and [8], [9]). The class-$\mathcal{D}$ kernels of the GWD are

$$g_{W(\rho)}(\eta)=\delta(\eta+\rho), \qquad G_{W(\rho)}(\xi)=e^{j2\pi\rho\xi}.$$

As the name indicates, the GWD may be considered to be a natural generalization of the WD; in particular, the WD is a special case obtained by setting $\rho=0$. Another well-known special case is the *Rihaczek distribution* (RD)

$$R_{x,y}(t,f) = \int_\tau x(t+\tau)y^*(t)\,e^{-j2\pi f\tau}d\tau = X(f)\,y^*(t)\,e^{j2\pi tf}$$

which is obtained for $\rho=1/2$. Note that the autoGWD is complex valued unless $\rho=0$, i.e., except for the special case of the WD.

A. GWD Representation of Shift-Scale Invariant BTFR's

The GWD family is significant in the context of the shift-scale invariant class $\mathcal{D}$ since *any shift-scale invariant BTFR T can be written as a (continuous) weighted superposition of GWD's*. Indeed, it is shown in [2] that

$$T\in\mathcal{D} \Leftrightarrow T_{x,y}(t,f)=\int_\eta g_T(-\eta)W^{(\eta)}_{x,y}(t,f)\,d\eta, \qquad (3.1)$$

where the kernel $g_T(\eta)$ of T plays the role of the superposition's weighting function except for a reversal of the η axis.

The superposition expression (3.1) indicates that the GWD is, in fact, the most basic BTFR type of the shift-scale invariant class $\mathcal{D}$. If we know the time-frequency localization properties of the GWD family, then, at least in principle, we are able to predict the time-frequency localization properties of an arbitrary shift-scale invariant BTFR by invoking (3.1). We shall therefore study the time-frequency localization properties of the GWD in the following.

B. Interference Geometry of the GWD

Although more general and more formal approaches may be used to analyze the GWD's time-frequency localization (especially the method of stationary phase and catastrophe-theoretical methods [8], [21]), we shall restrict our discussion to the consideration of some very simple examples. We start with a two-component signal whose energy is located around two points in the time-frequency plane. This situation may be formulated in a mathematically tractable manner, and it yields a fairly complete picture of the GWD's time-frequency localization.

Let $x(t)=x_1(t)+x_2(t)$, where

$$x_1(t)=(\mathbf{M}_{f_1}\mathbf{S}_{t_1}x_o)(t),\ x_2(t)=(\mathbf{M}_{f_2}\mathbf{S}_{t_2}x_o)(t) \qquad (3.2)$$

are two time-frequency shifted versions of a basic signal $x_o(t)$, which we assume to be concentrated around the origin of the time-frequency plane (e.g., a Gaussian signal). Evidently, the signals $x_1(t)$ and $x_2(t)$ will then be concentrated around the time-frequency points (t_1,f_1) and (t_2,f_2), respectively.

Like any other quadratic signal representation, the auto-GWD of the two-component signal $x(t)=x_1(t)+x_2(t)$ consists of two "signal" terms and one cross or "interference"

term

$$W^{(\rho)}_{x_1+x_2}(t,f) = W^{(\rho)}_{x_1}(t,f) + W^{(\rho)}_{x_2}(t,f) + I^{(\rho)}_{x_1,x_2}(t,f).$$

The signal terms $W^{(\rho)}_{x_1}(t,f)$ and $W^{(\rho)}_{x_2}(t,f)$ corresponding to the signal components $x_1(t)$ and $x_2(t)$ are the autoGWD's of $x_1(t)$ and $x_2(t)$, respectively. Due to (3.2) and the GWD's shift invariance, these signal terms are simply time-frequency shifted versions of $W^{(\rho)}_{x_0}(t,f)$

$$W^{(\rho)}_{x_1}(t,f) = W^{(\rho)}_{x_0}(t-t_1, f-f_1),$$
$$W^{(\rho)}_{x_2}(t,f) = W^{(\rho)}_{x_0}(t-t_2, f-f_2). \tag{3.3}$$

Hence, they are concentrated around the time-frequency points (t_1, f_1) and (t_2, f_2), respectively.

The interference term (IT) is obtained after a somewhat tedious calculation as follows [8]:

$$I^{(\rho)}_{x_1,x_2}(t,f) = W^{(\rho)}_{x_1,x_2}(t,f) + W^{(\rho)}_{x_2,x_1}(t,f) = \tag{3.4.a}$$
$$= F^{+}[t-(t_{12}-\rho\tau_{12}), f-(f_{12}+\rho\upsilon_{12})]$$
$$+ F^{-}[t-(t_{12}+\rho\tau_{12}), f-(f_{12}-\rho\upsilon_{12})]$$

where

$$F^{\pm}(t,f) = W^{(\rho)}_{x_0}(t,f)e^{\pm j[2\pi(\upsilon_{12}t-\tau_{12}f)+\varphi^{\pm}_{12}]} \tag{3.4.b}$$

with

$$\varphi^{\pm}_{12} = 2\pi\upsilon_{12}(t_{12} \mp \rho\tau_{12}). \tag{3.4.c}$$

Here, $t_{12} = (t_1+t_2)/2$ and $f_{12} = (f_1+f_2)/2$ denote the center time and center frequency between the "signal times" t_1, t_2 and "signal frequencies" f_1, f_2, respectively, whereas $\tau_{12} = t_1 - t_2$ and $\upsilon_{12} = f_1 - f_2$ are the corresponding time lag and frequency lag, respectively.

The signal terms and IT derived above are illustrated in Fig. 3. The results obtained may be summarized as follows:

(i) From (3.3), it is clear that the signal terms are correctly located around the time-frequency points (t_1, f_1) and (t_2, f_2), respectively, independent of the GWD parameter ρ.

(ii) From (3.4), we conclude that the IT consists of two oscillatory subterms located around the time-frequency points $(t_{12} - \rho\tau_{12}, f_{12} + \rho\upsilon_{12})$ and $(t_{12} + \rho\tau_{12}, f_{12} - \rho\upsilon_{12})$, respectively. The IT's distance from the center point (t_{12}, f_{12}) grows linearly with the GWD parameter's magnitude $|\rho|$. The IT oscillates in the time and frequency directions with "frequencies" $\upsilon_{12} = f_1 - f_2$ and $\tau_{12} = t_1 - t_2$, respectively. The overall IT oscillation will therefore be faster for increasing distance between the signals $x_1(t)$ and $x_2(t)$ in the time-frequency plane.

The special cases of the WD ($\rho = 0$) and RD ($\rho = 1/2$) are illustrated in Fig. 4. In the WD case, the two IT subterms coalesce into a single real-valued IT located around the center point (t_{12}, f_{12}). In the RD case, on the other hand, the signal terms and IT subterms form the corners of a rectangle. Evidently, the IT of the WD features the maximum time-frequency concentration among the entire GWD family. We note that a formal proof of the WD's optimality with respect to time-frequency concentration has been given in [9].

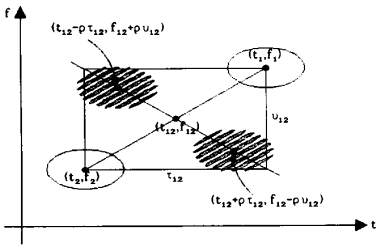

Fig. 3. Signal terms and interference term of the generalized WD. Schematic illustration for the two-component signal $x(t) = X_1(t) + X_2(t)$ with signal components $x_1(t) = M_{f_1}S_{t_1}x_o)(t)$ and $x_2(t) = (M_{f_2}S_{t_2}x_0)(t)$.

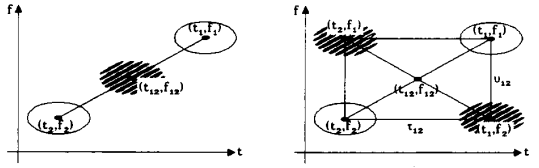

Fig. 4. Schematic illustration of the signal terms and interference term of (a) WD and (b) Rihaczek distribution for the two-component signal considered in Fig. 3.

C. Extension of Interference Geometry

The geometry of the GWDIT's discussed above was derived for a simple two-component signal. However, this geometry is, in fact, generally valid when interpreted in the following sense: Whenever a signal has energy around two different time-frequency points (t_1, f_1) and (t_2, f_2), the GWD will contain two "signal terms" around (t_1, f_1) and (t_2, f_2), respectively, and two oscillatory IT subterms around $(t_{12}-\rho\tau_{12}, f_{12}+\rho\upsilon_{12})$ and $(t_{12}+\rho\tau_{12}, f_{12}-\rho\upsilon_{12})$. We shall illustrate this principle for the WD ($\rho = 0$) and the RD ($\rho = 1/2$) using the example of a windowed chirp signal (linear frequency modulation)

$$x(t) = a(t)e^{j\pi ct^2}, \quad a(t) \geq 0, \quad c \in \mathbb{R}$$

where the window $a(t)$ is smooth and assumed to be effectively zero outside some interval $[t_a, t_b]$.

The WD is easily obtained as

$$W_x(t,f) = W_a(t, f-ct)$$

which, for sufficiently smooth $a(t)$, is well concentrated along the chirp signal's instantaneous-frequency line $f_{x,\mathrm{inst}}(t) = ct$ since $W_a(t,f)$ is concentrated around $f = 0$ for all $t \in [t_a, t_b]$. For the RD, on the other hand, application of the stationary-phase method [8] yields the approximation

$$R_x(t,f) \approx Ca(t)a\left(\frac{f}{c}\right)\exp\left[-j\frac{\pi}{c}(f-ct)^2\right]$$

where C is a constant factor. We see that the RD is oscillatory and effectively located inside the rectangle $[t_a, t_b] \times [ct_a, ct_b]$. The local oscillation around a time-frequency point grows faster with increasing distance between this point and the instantaneous-frequency line $f_{x,\mathrm{inst}}(t) = ct$.

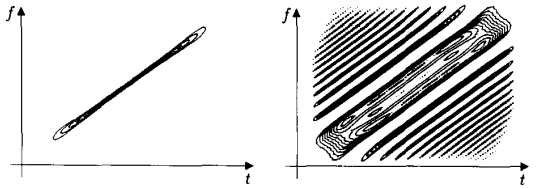

Fig. 5. Time-frequency representation of a windowed chirp signal: (a) WD; (b) real part of Rihaczek distribution.

Fig. 5 shows the WD and the (exact) RD. It is seen that the oscillatory RD parts located away from the instantaneous-frequency line can be interpreteted as interference terms obeying the geometric characteristics described by (3.4) (cf. Fig. 4(b)). Note that there are no separate IT's in the WD case since here, the IT component for any pair of signal points on the instantaneous-frequency line (the WD signal term) falls again onto this signal term (cf. Fig. 4(a)). This, of course, will be true only for a linear frequency modulation (where the instantaneous frequency corresponds to a straight line in the time-frequency plane).

This example shows that the GWD parameter ρ has a dramatic influence on the GWD's time-frequency localization and concentration. This may be explained by the fact that ρ controls the *location of the interference terms in the time-frequency plane*. The example also illustrates that $\rho = 0$ (the WD case) leads to optimum time-frequency concentration.

We finally mention that the IT's location (not, however, its oscillation) can also be inferred from the GWD's "interference formula"

$$|W_x^{(\rho)}(t,f)|^2 = \int_\tau \int_\upsilon W_x^{(\rho)}\left[t+\left(\frac{1}{2}+\rho\right)\tau, f+\left(\frac{1}{2}-\rho\right)\upsilon\right] \times W_x^{(\rho)*}\left[t-\left(\frac{1}{2}-\rho\right)\tau, f-\left(\frac{1}{2}+\rho\right)\upsilon\right] \times d\tau d\upsilon$$

as discussed further in [8].

IV. Shift-Scale Invariant Smoothing of the WD

After this discussion of the GWD family, we return to the study of a general shift-scale invariant BTFR T. Due to the superposition expression (3.1)

$$T_x(t,f) = \int_\eta g_T(-\eta) W_x^{(\eta)}(t,f) d\eta, \qquad (4.1)$$

we may hope to derive the time-frequency localization properties of any shift-scale invariant BTFR T from the simple properties of the GWD discussed in the previous section.

A. Potential Support of Interference Terms

To illustrate the underlying principle, we reconsider the basic situation of a two-component signal $x(t) = x_1(t) + x_2(t)$ whose components $x_1(t)$ and $x_2(t)$ are concentrated around the time-frequency points (t_1, f_1) and (t_2, f_2), respectively. Let us assume that the effective support of the kernel $g_T(\eta)$ is some interval $[-\eta_0, \eta_0]$. Then, combining the localization properties of the GWD (cf. Fig. 3) and the superposition (4.1), we obtain the following results:

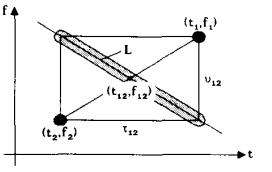

Fig. 6. Time-frequency localization of shift-scale invariant BTFR's: Time-frequency support of the signal terms and potential time-frequency support of the interference term (shaded region).

i) The signal terms of $T_x(t,f)$ are concentrated around the time-frequency points (t_1, f_1) and (t_2, f_2), respectively.
ii) The IT of $T_x(t,f)$, on the other hand, is formed by superposition of the IT's of all GWD's for which $\rho \in [-\eta_0, \eta_0]$. Hence, it will be located around the set L of points $(t_{12} - \eta\tau_{12}, f_{12} + \eta\upsilon_{12})$ with $\eta \in [-\eta_0, \eta_0]$. Obviously, L is a segment of a straight line passing through the center point (t_{12}, f_{12}) and bounded by the points $(t_{12} - \eta_0\tau_{12}, f_{12} + \eta_0\upsilon_{12})$ and $(t_{12} + \eta_0\tau_{12}, f_{12} - \eta_0\upsilon_{12})$.

This geometry is depicted in Fig. 6 for the case $\eta_0 = 1/2$. The essential conclusion is that the IT of a shift-scale invariant BTFR tends to be *spread out* over a larger region of the time-frequency plane (as compared to the WD). This spreading effect is stronger for a wider $g_T(\eta)$ (i.e., a larger η_0) and for a larger distance between the interfering signal components (larger $|\tau_{12}|$ and/or $|\upsilon_{12}|$). Again, the WD is seen to be the case of minimum IT spread since here, $g_W(\eta) = \delta(\eta)$ and thus $\eta_0 = 0$; in addition, the IT spread is here independent of $|\tau_{12}|$ and $|\upsilon_{12}|$.

Although the previous arguments are conceptually straightforward, a closer analysis will show that the results obtained must be used with caution. Specifically, the neigborhood of the line segment L should be interpreted as the *potential* support of the IT of $T_x(t,f)$ since the IT contributions from different GWD's (corresponding to different values of η) in the superposition (4.1) tend to cancel each other. Indeed, we shall see presently that this canceling effect will typically occur if the kernel $g_T(\eta)$ is sufficiently smooth.

B. Shift-Scale Invariant Smoothing of the WD

In order to establish this property, we recall that $T_x(t,f)$, being shift-invariant, can be derived from the WD by a convolution (cf. (2.1.c))

$$T_x(t,f) = \int_{t'} \int_{f'} \psi_{C,T}(t-t', f-f') W_x(t',f') dt' df'. \qquad (4.2)$$

Consequently, the Fourier transform of $T_x(t,f)$

$$\tilde{T}_x(\tau,\upsilon) \triangleq \int_t \int_f T_x(t,f) e^{-j2\pi(\upsilon t - \tau f)} dt df$$

is derived from the ambiguity function (AF) $A_x(\tau,\upsilon)$, which is the Fourier transform of the WD, by a multiplication (cf. (2.1.d))

$$\tilde{T}_x(\tau,\upsilon) = \Psi_{C,T}(\tau,\upsilon) A_x(\tau,\upsilon). \qquad (4.3)$$

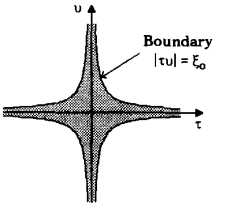

Fig. 7. Cross-shaped effective support of the weighting function $\Psi_{C,T}(\tau, \upsilon) = G_T(\tau\upsilon)$ of a shift-scale invariant smoothed WD.

The kernel $\Psi_{C,T}(\tau, \upsilon)$ is the Fourier transform of $\psi_{C,T}(t, f)$

$$\Psi_{C,T}(\tau, \upsilon) = \int_t \int_f \psi_{C,T}(t, f) e^{-j2\pi(\upsilon t - \tau f)} dt df.$$

This well-known result is valid for the Fourier transform of any shift-invariant BTFR. If the kernel $\psi_{C,T}(t, f)$ is a smooth function, then the convolution (4.2) actually amounts to a *smoothing* of the WD, and we shall then call T a *smoothed WD* (SWD). A smoothing of the WD is often used for attenuating the oscillatory ITs of the WD [8], [16], [1] or, in a stochastic framework, for reducing the WD's variance [17], [22]. Indeed, the smoothness condition implies that $\Psi_{C,T}(\tau, \upsilon)$, which is the Fourier transform of $\psi_{C,T}(t, f)$, is concentrated around the origin of the (τ, υ) plane, i.e., it decays for larger values of $|\tau|$ and/or $|\upsilon|$. Under this condition, the weighting (4.3) causes an attenuation of IT's since the IT's of the AF typically occur away from the origin of the (τ, υ) plane.

If, as we assume, the BTFR T is not merely shift-invariant but shift-scale invariant, then $\Psi_{C,T}(\tau, \upsilon) = G_T(\tau\upsilon)$ according to (2.3.d), and (4.3) finally becomes

$$\tilde{T}_x(\tau, \upsilon) = G_T(\tau\upsilon) A_x(\tau, \upsilon). \tag{4.4}$$

In the following, we also assume the normalization $G_T(0) = 1$, which, according to Table I, guarantees that T satisfies the marginal properties.

If $g_T(\eta)$ is sufficiently smooth (i.e., a low-pass function), then $G_T(\xi)$ will be effectively zero for $|\xi| > \xi_0$, where ξ_0 is the effective bandwidth of $g_T(\eta)$. This means that $\Psi_{C,T}(\tau, \upsilon) = G_T(\tau\upsilon) \approx 0$ for $|\tau\upsilon| > \xi_0$ and shows that T can be interpreted as a smoothed WD (SWD). The effective support of $\Psi_{C,T}(\tau, \upsilon)$ is a cross-shaped region of the (τ, υ) plane, as shown in Fig. 7 [11], [8], [20]. The specific type of WD smoothing produced by a product-type (cross-shaped) kernel $\Psi_{C,T}(\tau, \upsilon) = G_T(\tau\upsilon)$ will be called *shift-scale invariant smoothing*.

A prominent example of a shift-scale invariant SWD is the *Choi-Williams distribution* for which $G_T(\xi)$ is a Gaussian [11]

$$G_{\mathrm{CWD}}(\xi) = e^{-(2\pi\xi)^2/\sigma}.$$

In [20], the family of "reduced-interference" distributions is introduced as a class of shift-scale invariant SWD's with the kernel $G_T(\xi)$ constrained such that many desirable mathematical properties are satisfied.

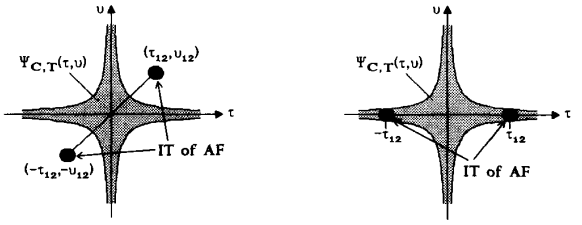

Fig. 8. Ambiguity-domain analysis of the IT attenuation in a shift-scale invariant smoothed WD: (a) Signal components occurring at different times($\tau_{12} \neq 0$) and different frequencies ($\upsilon_{12} \neq 0$); (b) signal components occurring around the same frequency ($\upsilon_{12} \approx 0$).

C. Ambiguity-Domain Analysis of Shift-Scale Invariant SWD's

In order to understand the peculiarities of shift-scale invariant smoothing, we once again return to our two-component signal whose components are concentrated around the time-frequency points (t_1, f_1) and (t_2, f_2). It is easily shown that the IT of the AF is here concentrated around the points $(\tau_{12}, \upsilon_{12})$ and $(-\tau_{12}, -\upsilon_{12})$ of the (τ, υ) plane, where $\tau_{12} = t_1 - t_2$ and $\upsilon_{12} = f_1 - f_2$ as before. Now, if $|\tau_{12}\upsilon_{12}|$ is sufficiently larger than ξ_0, which is the effective bandwidth of $g_T(\eta)$, then it follows from (4.4) that the IT in $\tilde{T}_x(\tau, \upsilon)$, and thus the IT in the original shift-scale invariant SWD $T_x(t, f)$ as well, will be effectively suppressed. This situation is illustrated in Fig. 8(a).

The condition $|\tau_{12}\upsilon_{12}| > \xi_0$, which was seen above to produce good IT attenuation, will be violated if either $\tau_{12} \approx 0$ or $\upsilon_{12} \approx 0$. The first case occurs when $t_1 \approx t_2$, i.e., when the two interfering signal components occur around the same time. The second case arises when $f_1 \approx f_2$, i.e., when the two signal components occur around the same frequency. In these cases, the attenuation of IT's will be poor since the AF's IT is now near the τ axis or the υ axis, where $\Psi_{C,T}(\tau, \upsilon) \approx G_T(0) = 1$. The case $\upsilon_{12} \approx 0$ is illustrated in Fig. 8(b).

This discussion shows that the IT attenuation achieved by a shift-scale invariant SWD is extremely sensitive to the relative time-frequency location of the interfering signal components. Satisfactory IT attenuation will be obtained only if the signal components do not occur either around the same time or around the same frequency. Fig. 9 demonstrates this sensitivity by showing the results of the Choi–Williams distribution for the two situations considered in Fig. 8.

D. Spreading of Interference Terms

Additional insights are obtained by studying a two-component signal with Dirac components $x_1(t) = \delta(t - t_1)$ and $x_2(t) = \delta(t - t_2)$. The shift-scale invariant BTFR $T_x(t, f)$ consists of the signal terms

$$T_{x_1}(t, f) = \delta(t - t_1), \qquad T_{x_2}(t, f) = \delta(t - t_2)$$

and the IT

$$I_{x_1,x_2}(t, f) = \frac{1}{|\tau_{12}|}\left[g_T\left(\frac{t - t_{12}}{\tau_{12}}\right)e^{-j2\pi\tau_{12}f} + g_T\left(-\frac{t - t_{12}}{\tau_{12}}\right)e^{j2\pi\tau_{12}f}\right]. \tag{4.5}$$

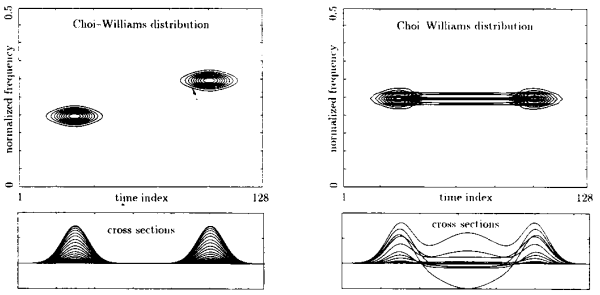

(a) (b)

Fig. 9. Choi–Williams distribution (with $\alpha = 10$) of a two-component signal consisting of two time-frequency shifted Gaussians: (a) Signal components occurring at different times and frequencies; (b) signal components occurring at the same frequency.

The AF is depicted in Fig. 10(a), and the SWD result $T_x(t,f)$ is plotted in Fig. 10(b) for the special case of the Choi–Williams distribution. Since the two AF signal terms lie exactly on the υ axis where $\Psi_{C,T}(\tau,\upsilon) = G_T(0) = 1$, they are not affected by the weighting by $\Psi_{C,T}(\tau,\upsilon)$; as a consequence, the signal terms of $T_x(t,f)$ equal the signal terms of the WD and thus feature perfect time concentration. The IT, on the other hand, is spread out in time as predicted by (4.5). According to (4.5), this spreading is stronger for a wider $g_T(\eta)$ and a larger time distance $|\tau_{12}| = |t_1 - t_2|$ between the two impulses. This behavior agrees with the results derived from the GWD superposition formula (4.1) at the beginning of this section. Alternatively, the IT spreading may also be viewed as a consequence of the truncation of the AF's IT by the weighting (cf. Fig. 10(a)).

The condition $G_T(0) = 1$ assuring the marginal properties implies $\int g_T(\eta)d\eta = 1$; as a consequence, the integral of the IT (4.5) over time is easily shown to be the cosine

$$\int_t I_{x_1,x_2}(t,f)dt = 2\cos(2\pi\tau_{12}f)$$

which equals the result obtained for the WD. Hence, as far as the IT's time integral is concerned, the IT is not attenuated at all. Here, we have a situation where the IT is spread out according to (4.1), but the various IT components do *not* cancel each other. While the IT's height is reduced (as compared to the WD), the IT's spread is increased in proportion such that the IT's time integral remains the same. This kind of behavior will always be observed if the signal components are not disjoint in frequency. Of course, dual results can be obtained for signal components that are not disjoint in time.

E. Time-Frequency Concentration

The previous example has also shown that $T_x(t,f) = \delta(t-t_0)$ for $x(t) = \delta(t-t_0)$. The fact that the signal's perfect time concentration is preserved here seems to imply that shift-scale invariant SWD's have perfect time resolution. However, it should be clear from the ambiguity-domain analysis (cf. Fig. 10(a)) that the ideal Dirac impulse $x(t) = \delta(t - t_0)$ and the dual signal $x(t) = e^{j2\pi f_0 t}$ (a Dirac impulse in the frequency domain) are the *only* signals whose time or

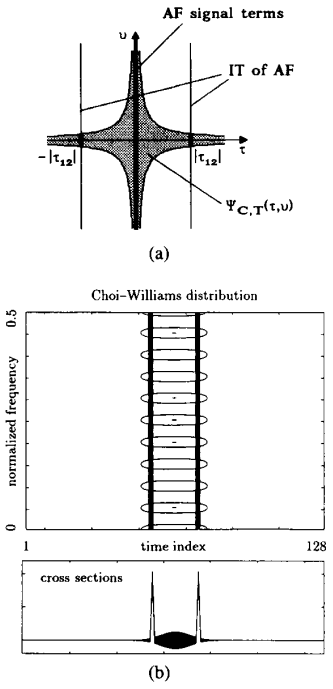

Fig. 10. Shift-scale invariant SWD of the two-component signal $x(t) = \delta(t - t_1) + \delta(t - t_2)$: (a) Ambiguity-domain analysis; (b) Choi–Williams distribution with $\alpha = 5$.

frequency concentration is preserved in a shift-scale invariant SWD. In *all* other cases, the multiplication of the AF by the weighting function $\Psi_{C,T}(\tau,\upsilon)$ will effect a truncation of the AF, which leads to a broadening of $T_x(t,f)$ as compared to the WD and thus causes a loss in time-frequency concentration.

We illustrate this broadening effect by considering the infinite-length chirp signal

$$x(t) = e^{j\pi ct^2}, \qquad c \in \mathbb{R}$$

whose WD $W_x(t,f) = \delta(f - ct)$ is perfectly concentrated along the instantaneous-frequency line $f_{x,\text{inst}}(t) = ct$. The AF is $A_x(\tau,\upsilon) = \delta(\upsilon - c\tau)$, which leads to the situation depicted in Fig. 11(a). The weighting function $\Psi_{C,T}(\tau,\upsilon) = G_T(\tau\upsilon)$ is seen to cause a truncation of the AF. The resulting time-frequency concentration loss in the shift-scale invariant SWD is illustrated in Fig. 11(b) for a finite-length (windowed) chirp signal.

For a rough analysis of the concentration loss, we assume the particularly simple weighting function corresponding to an idealized cutoff, i.e., a rectangular $G_T(\xi)$

$$G_T(\xi) = \begin{cases} 1, & |\xi| < \xi_0 \\ 0, & |\xi| > \xi_0 \end{cases}. \tag{4.6}$$

The Fourier transform of $T_x(t,f)$ is obtained as

$$\begin{aligned} \widetilde{T}_x(\tau,\upsilon) &= G_T(\tau\upsilon)A_x(\tau,\upsilon) = G_T(\tau\upsilon)\delta(\upsilon - c\tau) \\ &= G_T(c\tau^2)\delta(\upsilon - c\tau) \end{aligned} \tag{4.7}$$

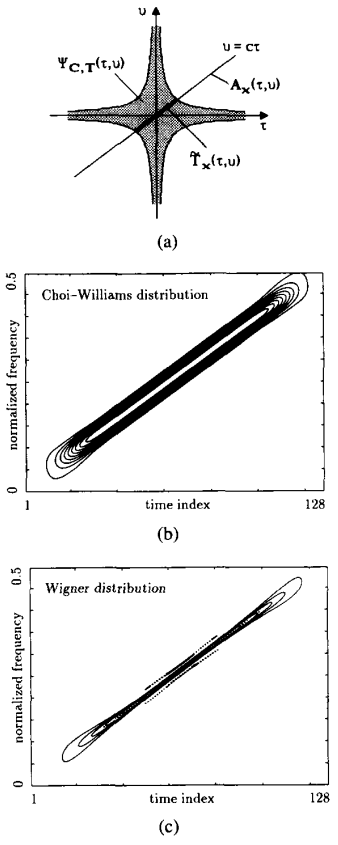

Fig. 11. Shift-scale invariant SWD of a chirp signal: (a) Ambiguity-domain analysis; (b) Choi–Williams distribution with $\alpha = 10$; (c) WD for comparison.

and we easily obtain from (4.6) and (4.7)

$$T_x(t,f) = \frac{1}{\upsilon_0}\,\mathrm{sinc}\left(\frac{f-ct}{\upsilon_0}\right), \qquad \upsilon_0 = \frac{1}{2}\sqrt{\frac{|c|}{\xi_0}}$$

where $\mathrm{sinc}\ \alpha = \sin(\pi\alpha)/(\pi\alpha)$. We see that the shift-scale invariant SWD $T_x(t,f)$ is still concentrated along the instantaneous-frequency line, but the concentration is not perfect; specifically, the frequency width is proportional to the parameter υ_0, which grows with decreasing cut-off parameter ξ_0.

This example shows that a small value of ξ_0 (which will produce good IT attenuation) results in poor time-frequency concentration. This tradeoff between good IT attenuation and good time-frequency concentration is inherent in any SWD be it shift-scale invariant or not.

V. Conclusion

The class of shift-scale invariant BTFR's comprises all BTFR's that are "invariant" to time shifts, frequency shifts, and time-frequency scalings. Hence, this class forms the intersection of the shift-invariant (Cohen) class and the affine class, and it contains BTFR's that are interesting either from a formal viewpoint (e.g., the family of generalized WD's) or from a practical viewpoint (e.g., the Choi–Williams distribution). While BTFR's of Cohen's class or the affine class are generally characterized by 2-D kernel functions, a 1-D kernel function suffices in the special case of shift-scale invariant BTFR's.

This paper concentrated on the time-frequency localization properties of shift-scale invariant BTFR's. Since any such BTFR is a superposition of GWD's, the family of GWD's was studied in some detail, and it was shown that the WD is the GWD whose IT's feature maximum time-frequency concentration.

Motivated by the practical importance of attenuating the IT's of the WD by means of a smoothing operation, we next investigated the localization properties of those shift-scale invariant BTFR's that can be viewed as smoothed WD's (e.g., the Choi–Williams distribution). It was here found that the shift-scale invariant structure is a mixed blessing. An advantage of shift-scale invariant smoothed WD's is the fact that they are capable of retaining some of the nice mathematical properties of the WD, which are usually lost when some other type of smoothing is used. However, the price paid is a characteristic sensitivity of IT attenuation to the time-frequency locations of the signal components. A simple analysis in the "ambiguity domain" shows that IT's will be poorly attenuated if the corresponding signal components occur either around the same time or around the same frequency. In these cases, the reduction of IT height is compensated by a proportional increase of IT spread. It was furthermore demonstrated that like any other type of smoothing, a shift-scale invariant smoothing causes a loss in time-frequency concentration (except for the somewhat academic case of an ideal Dirac impulse in the time or frequency domain).

We finally note that further aspects of shift-scale invariant BTFR's (which are related to the BTFR properties of regularity and unitarity) are discussed in [23].

Acknowledgment

The authors wish to thank A. Papandreou for contributing the Choi–Williams distribution plots in Figs. 9–11.

References

[1] F. Hlawatsch and G. F. Boudreaux-Bartels, "Linear and quadratic time-frequency signal representations," *IEEE Signal Processing Mag.*, vol. 9, no. 2, pp. 21–67, Apr. 1992.
[2] F. Hlawatsch, "Duality and classification of bilinear time-frequency signal representations," *IEEE Trans. Signal Processing*, vol. 39, no. 7, pp. 1564–1574, July 1991.
[3] L. Cohen, "Generalized phase-space distribution functions," *J. Math. Phys.*, vol. 7, pp. 781–786, 1966.
[4] ——, "Distributions in signal theory," in *Proc. 1984 IEEE Int. Conf. Acoust. Speech Signal Processing (ICASSP–84)* (San Diego, CA), Mar. 1984, pp. 41.B.1.1–4.
[5] O. Rioul and P. Flandrin, "Time-scale energy distributions: A general class extending wavelet transforms," *IEEE Trans. Signal Processing*, vol. 40, no. 7, pp. 1746–1757, July 1992.
[6] J. Bertrand and P. Bertrand, "Affine time-frequency distributions," in *Time-Frequency Signal Analysis—Methods and Applications* (B. Boashash, Ed.). Melbourne, Australia: Longman-Cheshire, 1991.
[7] T. A. C. M. Claasen and W. F. G. Mecklenbräuker, "The Wigner distribution—A tool for time-frequency signal analysis," Parts I–III, *Philips J. Res.*, vol. 35, pp. 217–250, 276–300, 372–389; 1980.
[8] F. Hlawatsch and P. Flandrin, "The interference structure of the Wigner distribution and related time-frequency signal representations," to ap-

pear in *The Wigner Distribution—Theory and Applications in Signal Processing* (W. Mecklenbräuker, Ed.). New York: Elsevier, 1994.
[9] A. J. E. M. Janssen, "On the locus and spread of pseudo-density functions in the time-frequency plane," *Philips J. Res.*, vol. 37, pp. 79–110, 1982.
[10] L. Cohen, "Time-frequency distributions—A review," *Proc. IEEE*, vol. 77, no. 7, pp. 941–981, July 1989.
[11] H. -I. Choi and W. J. Williams, "Improved time-frequency representation of multicomponent signals using exponential kernels," *IEEE Trans. Acoust. Speech Signal Processing*, vol. ASSP-37, pp. 862–871, June 1989.
[12] R. A. Altes, "Detection, estimation, and classification with spectrograms," *J. Acoust. Soc. Amer.*, vol. 67, pp. 1232–1246, Apr. 1980.
[13] S. Kadambe and G. F. Boudreaux-Bartels, "A comparison of the existence of "cross terms" in the Wigner distribution and the squared magnitude of the wavelet transform and the short time Fourier transform," *IEEE Trans. Signal Processing*, vol. 40, no. 10, pp. 2498–2517, Oct. 1992.
[14] C. H. Page, "Instantaneous power spectra," *J. Appl. Phys.*, vol. 23, pp. 103–106, 1952.
[15] M. J. Levin, "Instantaneous power spectra and ambiguity function," *IEEE Trans. Inform. Theory*, vol. IT–13, pp. 95–97, 1967.
[16] P. Flandrin, "Some features of time-frequency representations of multicomponent signals," in *Proc. IEEE 1984 Int. Conf. Acoust. Speech Signal Processing (ICASSP-84)* (San Diego, CA), Mar. 1984, pp. 41B.4.1–41B.4.4.
[17] W. Martin and P. Flandrin, "Wigner-Ville spectral analysis of nonstationary processes," *IEEE Trans. Acoust. Speech Signal Processing*, vol. ASSP-33, no. 6, pp. 1461–1470, Dec. 1985.
[18] D. L. Jones and T. W. Parks, "A resolution comparison of several time-frequency representations," *IEEE Trans. Signal Processing*, vol. 40, no. 2, pp. 413–420, Feb. 1992.
[19] F. Hlawatsch, "A study of bilinear time-frequency signal representations, with applications to time-frequency signal synthesis," Ph.D. dissertation, Technische Universität Wien, Vienna, Austria, 1988.
[20] J. Jeong and W. J. Williams, "Kernel design for reduced interference distributions," *IEEE Trans. Signal Processing*, vol. 40, no. 2, pp. 402–412, Feb. 1992.
[21] P. Flandrin and F. Hlawatsch, "Signal representations geometry and catastrophes in the time-frequency plane," in *Mathematics in Signal Processing* (T. S. Durrani et al., Eds.). Oxford: Clarendon, 1987, pp. 3–14.
[22] P. Flandrin and W. Martin, "The Wigner-Ville spectrum of nonstationary random signals," to appear in *The Wigner Distribution—Theory and Applications in Signal Processing* (W. Mecklenbräuker, Ed.). New York: Elsevier, 1994.
[23] F. Hlawatsch, "Regularity and unitarity of bilinear time-frequency signal representations," *IEEE Trans. Inform. Theory*, vol. 38, pp. 82–94, Jan. 1992.

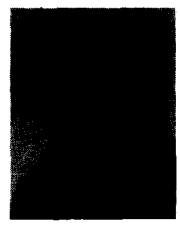

Franz Hlawatsch (S'85–M'88) received the Diplom-Ingenieur and Dr. techn. degrees in electrical engineering from the Vienna University of Technology, Vienna, Austria, in 1983 and 1988, respectively.

Since 1983, he has been a Research and Teaching Assistant at the Department of Communications Engineering of the Vienna University of Technology. During 1991–1992, he spent a sabbatical year with the Department of Electrical Engineering at the University of Rhode Island. His research interests are mainly in signal theory and signal processing with emphasis on time-frequency methods.

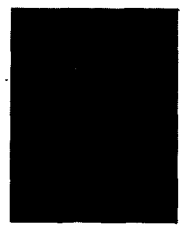

Rüdiger L. Urbanke received the Diplom-Ingenieur degree in electrical engineering from the Vienna University of Technology, Vienna, Austria, in 1990. In 1992, as a recipient of a Fulbright Fellowship, he received the M.S. degree in electrical engineering from Washington University, where he is currently enrolled as a Ph.D. student under a Donald F. Wann Fellowship.

In 1991, he was a Research and Teaching Assistant at the Department of Communications Engineering of the Vienna University of Technology. His research interests include signal processing, coding theory, and multiple-access communications.